Deployment of *n*-strut Cylindrical Tensegrity Booms

Kaan Yildiz[1] and George A. Lesieutre[2]

[1]Istanbul Technical University, Istanbul, Turkey 34469

[2]The Pennsylvania State University, University Park, Pennsylvania, USA, 16802

ABSTRACT

In this paper, general methods for the analysis of deployment of *n*-strut cylindrical Class-1 and Class-2 tensegrity booms are developed. Investigation of the geometries of cylindrical Class-1 and Class-2 tensegrity booms leads to comprehensive procedures for the deployment of cylindrical tensegrity booms with an arbitrary number (n) of struts in each stage. For Class-1 tensegrity booms, equilibrium surfaces that show the collection of feasible azimuth and declination angle pairs corresponding to self-equilibrated geometries are obtained numerically. Deployment is achieved by varying the azimuth and declination angle parameters while remaining on this equilibrium surface. For Class-2 tensegrity booms, two deployment strategies, one with constant-length reinforcing cables and another with actively controlled reinforcing cables, are considered, and deployment is achieved by varying the length of certain cables. Deployment is studied in detail for tensegrity booms with four struts in each stage and the results are presented. The developed generalization procedures for analyzing the geometry and deployment of *n*-strut cylindrical tensegrity booms makes it possible to address design concerns such as packaging efficiency, stiffness and stiffness-to-mass ratio.

[1]Postdoctoral Researcher, Aerospace Research Center and Faculty of Aeronautics and Astronautics, email: yildizkaa@gmail.com

[2]Associate Dean for Research and Graduate Programs, College of Engineering, 102B Hammond Building

INTRODUCTION

Tensegrity structures have received attention from several application fields such as the aerospace industry, civil engineering, and biology since their conception in the 1950s for architectural purposes. They are pre-stressed, pin-jointed structural frameworks that consist solely of axial load-carrying members, namely cables and struts. Connections between elements are via frictionless ball joints, and self-equilibrium of the structure is satisfied by the pre-stress.

In the aerospace engineering field, tensegrity structures are considered to be good candidates for deployable space structures (Furuya 1992; Motro 2003). They have reduced complexity compared to alternative deployable structure concepts since complicated joints between members are not present (Sultan and Skelton 1998). Furthermore, they are lightweight and ideally, bending loads are not experienced by individual members. Therefore, tensegrity structures fail mainly by cable yielding or strut buckling (Skelton and de Oliveira 2009).

Tensegrity structures are classified based on the maximum number of struts connected to each other at a single node (Skelton and de Oliveira 2009). If there is no direct connection between struts in a tensegrity structure, then it is called a *Class-1* tensegrity, the "classical" version. On the other hand, if the maximum number of struts connected to each other at a single node is k, then the structure is called a *Class-k* tensegrity structure. Class-1 and Class-k tensegrity structures offer different advantages and disadvantages. Most importantly, Class-1 tensegrity structures have better packaging capabilities, however, they exhibit lower stiffness. On the other hand, Class-k tensegrity structures are superior to Class-1 tensegrity structures in terms of stiffness, yet have inferior packaging capabilities (Masic et al. 2006; Dalilsafaei et al. 2012).

Deployment of a space boom can be defined as longitudinal extension of a boom from a compact stowed state to a longer operational state. The first study on deployment of tensegrity structures was reported by Furuya (Furuya 1992). Furuya conceptually investigated the deployment of tensegrity structures which were built by assembling small tensegrity units with connected struts. Double-layer tensegrity grids were considered by Hanaor (Hanaor 1993) as two-dimensional deployable space structures. Sultan and Skelton (Sultan and Skelton 1998; Sultan and Skelton 2003) studied

deployment of Class-1 tensegrity booms using cable actuation with no strut-to-strut connection. Similar tensegrity booms were studied by Tibert and Pellegrino (Tibert and Pellegrino 2003) by employing the idea of strut folding, and controlling the rate of deployment with a telescopic strut. They also distinguished between cable and strut actuation deployment modes, and pointed out the advantages of each.

The tensegrity boom studied by Furuya was also studied by Pinaud et al. (Pinaud et al. 2004) with an attempt to improve stiffness using constant-length reinforcing cables. The reinforcing cables were introduced to the structure which serve the purpose of locking the infinitesimal mechanisms that are present in the structure. The reinforcing cables have constant length as they are not actively controlled, and therefore the number of actuators is not increased. However, the use of constant-length reinforcing cables limits the achievable deployment range.

Michelletti and Williams (Micheletti and Williams 2007) developed a marching procedure for the form-finding problem for tensegrity structures which also can be used to study deployment and/or reconfiguration of tensegrity structures. Other interesting works devoted to deployment of tensegrity structures include inflatable tensegrity structures applications by Murata et al. (Murata et al. 2005) and Russell and Tibert (Russell and Tibert 2008) and footbridge applications for pedestrians by Rhode-Barbarigos et al. (Rhode-Barbarigos et al. 2010). Rhode-Barbarigos et al. parametrically designed tensegrity footbridges that consist of ring-modules with different number of struts, conducted structural analyses and made a comparison based on a structural efficiency index defined by Vu et al. (Vu et al. 2006) which takes design loads, self-weight, span and maximum deflection into account. In a following paper (Rhode-Barbarigos et al. 2012), deployment of pentagonal ring modules for tensegrity footbridge application was studied. The deployment was achieved by actively adjusting cable lengths and a deployment path which requires fewer actuators was also presented. In the proposed deployment strategy, they also took advantage of continuous "x" cables to reduce the number of actuators even further. Another work by Sychterz and Smith (Sychterz and Smith 2017) evaluated the influence of friction in the deployment of the tensegrity footbridge and developed a modified dynamic relaxation method to include these effects. Their

work revealed the significance of the friction and identified its most important trigger mechanism as the cable angle.

Sultan discussed the relation between the deployment time and energy loss during deployment which results from kinetic tendon damping (Sultan 2014). Sultan argued that damping is thermodynamically irreversible and may result in undesirable thermal effects such as damaging cables. He proposed that a deployment method is possible which exploits the infinitesimal mechanisms found in the structure. In this way, the energy loss becomes zero while the deployment path is tangent to the directions of infinitesimal mechanisms. As a result, it is possible to minimize the energy loss while eliminating the dependence on quasi-static deployment. Recently, Gonzalez et al. investigated the asymmetric reconfiguration of a three-strut cylindrical tensegrity structure along the directions of infinitesimal mechanisms (González et al. 2019).

The studies devoted to deployment of cylindrical tensegrity structures for deployable boom applications are mostly limited to cases having three struts in each stage. However, increasing the number of struts in each stage may yield advantages such as improved stiffness in particular directions (Yildiz and Lesieutre 2019). Yildiz and Lesieutre investigated two-stage cylindrical Class-2 tensegrity booms and showed that for fixed prestress forces in the struts, the maximum bending and shear rigidities for the booms were obtained with four struts in each stage. Furthermore, the axial rigidity was found to be maximum with three struts in each stage while the torsional rigidity increased with increasing number of struts. Therefore, in this paper generalization methods to design and deploy cylindrical Class-1 and Class-2 tensegrity booms are addressed. The number of struts in each stage can be selected arbitrarily ($n \geq 3$) and deployment using cable actuation can be simulated with the assumption of quasi-static motion, which allows velocity and acceleration effects to be neglected in the analysis (Sultan and Skelton 2003; Rhode-Barbarigos et al. 2012). The present research primarily aims to extend the work of Sultan and Skelton (Sultan and Skelton 1998; Sultan and Skelton 2003), and Pinaud et al. (Pinaud et al. 2004) in terms of deployment performance.

The mechanical performance of tensegrity structures depends not only on the axial stiffnesses

of individual members but also the level of prestress forces. The prestress forces present in the structure introduce geometric nonlinearity to tensegrity structures and contribute to the mechanical performance of the structure. Therefore, to account for the prestress and its effects, nonlinear models are widely used (Kebiche et al. 1999; Murakami 2001; Guest 2011). However, detailed analyses using these nonlinear models are usually expensive in terms of computational power and time. To avoid these expensive computational methods, *continuum beam modeling* techniques that allow for rapid approximation of the global behavior and comparison of stiffness were developed (Kebiche et al. 2008; Yildiz and Lesieutre 2019; Liu et al. 2019). Thus, to design tensegrity structures and evaluate their mechanical performance thoroughly, structural optimization (sizing and prestress) should be addressed. However, these are beyond the scope of this paper, and the focus is given to generalization of deployment.

This paper is organized as follows: First, general cylindrical tensegrity structures are briefly reviewed, and Class-1 and Class-2 tensegrity booms are examined. Then, deployment of cylindrical Class-1 and Class-2 tensegrity booms is addressed. The generalization of deployment of cylindrical tensegrity booms with n struts in each stage is achieved by identifying a pattern for nodal locations and defining a connectivity chart that includes member types. Finally, examples of deployment of Class-1 and Class-2 tensegrity booms are provided.

CYLINDRICAL TENSEGRITY STRUCTURES

Cylindrical tensegrity structures are special kinds of tensegrity structures that resemble a cylinder. Generally speaking, they have horizontal top and bottom planes, and the nodes lie at a constant radius from the axis centerline. Cylindrical tensegrity structures consisting of only one unit are named after the number of struts as *n-plex* tensegrity units. Therefore, a cylindrical tensegrity structure with three struts is a triplex, one with four struts is a quadruplex, and another with five struts is a pentaplex, etc. Typically, tensegrity booms are constructed by stacking cylindrical tensegrity units on top of each other.

A single cylindrical tensegrity unit (one stage of a cylindrical tensegrity boom) comprises of n struts and $3n$ cables. The horizontal planes are created by n top and n bottom cables. These

two horizontal planes are connected to each other with n "vertical cables" and n struts. This is the minimum number of elements required to generate a self-equilibrated cylindrical tensegrity unit, called as *minimal regular tensegrity prism* by Skelton and Oliveira (Skelton and de Oliveira 2009). The total number of nodes found in a cylindrical tensegrity unit is then $2n$, which are evenly spaced along the edges of the horizontal top and bottom planes. The nodes in each plane generate a regular polygon with n corners and the structure exhibits rotational symmetry. In order to satisfy prestressability conditions, the relative angle between the top and bottom planes should have a specific value, called the *twist angle* which is $\alpha = \pi/2 - \pi/n$ (Connelly and Terrell 1995; Masic and Skelton 2003; Estrada 2007). A cylindrical tensegrity unit with six struts, called a *hexaplex*, is shown in Fig. 1.

Cylindrical tensegrity units have been investigated by other researchers for specific numbers of struts, n, and cataloged. Analytical solutions and numerical calculations of the form finding problem and self-equilibrium equations are available in the literature (Pugh 1976; Murakami and Nishimura 2001; Estrada 2007). The focus of this paper, however, is the generalization of cylindrical Class-1 and Class-2 tensegrity booms constructed with cylindrical tensegrity units, their deployment, and qualitative comparison.

Class-1 Tensegrity Booms

Cylindrical Class-1 tensegrity booms can be constructed by stacking cylindrical tensegrity units on top of each other without creating a direct connection between struts. In a two-stage example, the top plane of the upper stage is the same regular polygon as the bottom plane of the lower stage, rotated 180° around the longitudinal axis. The bottom ends of the top-stage struts are located at the mid points of the horizontal cables of the top of the bottom stage, and the top ends of the bottom-stage struts are located at the mid points of the horizontal cables of the bottom of the top stage. The horizontal cables are thus combined, divided by struts, and they become *saddle cables* (Murakami and Nishimura 2001). Saddle cables generate a regular polygon with $2n$ corners in the xy plane. Additionally, diagonal cables are introduced to the structure in order to satisfy the requirements for a self-equilibrated geometry (Murakami and Nishimura 2001). A two-stage, three-strut cylindrical

Class-1 tensegrity boom is shown in Fig. 2.

In Fig. 2, in order to distinguish between different types of elements, they are shown with different colored lines. Black, blue, magenta, teal, and thick red lines represent top and bottom, vertical, saddle, diagonal cables, and struts, respectively.

Fig. 2(a) shows the regular polygons created by top, bottom, and saddle cables. Since the structure has three struts in each stage, equilateral triangles are formed in the top and bottom planes, and a regular hexagon is formed in the intersection level. Fig. 2(b) shows the four different levels in the structure: top, bottom, lower intersection, and upper intersection levels. The vertical distance between the intersection levels are known as *the overlap*, and a non-zero value is required to satisfy the prestressability conditions, as described in the next sections.

Class-2 Tensegrity Booms

Cylindrical Class-2 tensegrity booms can be constructed by stacking cylindrical tensegrity units on top of each other in such a way that struts are connected at nodes. In a two-stage example, the top plane of the upper stage is the same regular polygon as the bottom plane of the lower stage. Generally speaking, the same cylindrical tensegrity units are placed in an alternating clockwise and anticlockwise sense in order to maintain symmetry in the xy plane and minimize global extension-torsion coupling. The horizontal cables are combined at the intersection of two units and they are called *saddle cables*. Saddle cables generate the same regular polygon as in the top and bottom levels, rotated around the longitudinal axis by a twist angle that depends on the number of struts. Furthermore, optional reinforcing cables can be introduced to the structure which may serve two purposes: increasing stiffness and increasing design flexibility (Pinaud et al. 2004).

The addition of extra members achieves the former by locking the infinitesimal mechanisms (or soft modes) which are normally only stiffened to some extent by the introduced prestress (Nishimura 2000). These mechanisms or soft modes can be completely eliminated by the addition of extra elements and as a result, the structure yields higher stiffness. The latter is obtained by allowing a feasible range for twist angle, rather than a fixed value (Pinaud et al. 2004). Then, the twist angle can be treated as a design variable in optimization problems (Yildiz 2018). A two-stage, three-strut

cylindrical Class-2 tensegrity boom is shown in Fig. 3.

In Fig. 3, in order to distinguish between different types of elements, they are shown with different colored lines. Black, blue, magenta, dashed orange, and thick red lines represent top and bottom, vertical, saddle, reinforcing (optional) cables, and struts, respectively. Reinforcing cables between different levels connect nodes in a circumferential direction opposite to that of the vertical cables, as shown in Fig. 3(a).

Fig. 3(a) shows the regular polygons created by the top, bottom, and saddle cables. Since the structure has three struts in each stage, equilateral triangles are formed at each level. Fig. 3(b) shows the three different levels in the structure: top, bottom, and intermediate levels.

DEPLOYMENT OF CYLINDRICAL CLASS-1 TENSEGRITY BOOMS

Deployment of two-stage cylindrical Class-1 tensegrity booms with three struts in each stage was studied analytically by Sultan and Skelton (Sultan and Skelton 2003). They realized that the geometry of symmetrical cylindrical two-stage Class-1 tensegrity booms, also known as SVD ("Saddle-Vertical-Diagonal") tensegrity booms, can be represented by three independent parameters: azimuth angle, declination angle, and overlap (the vertical distance between the nodes at the intersection of two units, for instance the vertical distance between nodes 5 and 11 in Fig. 2(b)).

Then, the equilibrium matrix of the structure can be represented in terms of these parameters, and the prestressability conditions can be written as follows:

$$\mathbf{A}(\alpha, \delta, h)\mathbf{T} = \mathbf{0} \tag{1}$$

where α, δ, and h are the azimuth angle, the declination angle, and the overlap, respectively. The existing rotational symmetry within the structure imposes the azimuth angles to differ by 60° in the three-strut case, while the declination angle is the same for all struts. In Equation 1, $\mathbf{T}$ is the normalized force vector of the saddle, vertical, and diagonal cables. The equilibrium matrix, $\mathbf{A}$, is defined by Sultan and Skelton (Sultan and Skelton 2003) as follows:

$$\mathbf{A} = \begin{bmatrix} \frac{\partial S}{\partial \alpha} & \frac{\partial V}{\partial \alpha} & \frac{\partial D}{\partial \alpha} \\ \frac{\partial S}{\partial \delta} & \frac{\partial V}{\partial \delta} & \frac{\partial D}{\partial \delta} \\ \frac{\partial S}{\partial h} & \frac{\partial V}{\partial h} & \frac{\partial D}{\partial h} \end{bmatrix} \tag{2}$$

where S, V, and D are the lengths of saddle, vertical, and diagonal cables, respectively. Expressions for S, V, and D are given by Sultan and Skelton (Sultan and Skelton 2003) for the three-strut case, and omitted here for conciseness. The non-trivial solution to the prestressability condition can be obtained from

$$det(\mathbf{A}(\alpha, \delta, h)) = 0 \tag{3}$$

The solution to Equation 3 yields the overlap value as a function of azimuth and declination angles. Further, the normalized force vector, $\mathbf{T}$, can also be obtained from Equation 3 as explained by Sultan and Skelton (Sultan and Skelton 2003). The solutions can be represented by equilibrium surfaces with respect to overlap and total height of the structures, generated by feasible pairs of azimuth and declination angles that satisfy the prestressability conditions. Then, deployment–that is, vertical extension of the boom–can be achieved by selecting appropriate initial and final points on the equilibrium surface, typically assuming a linear path of sequential equilibrium states between them, and varying the parameters correspondingly. As the azimuth and declination angles vary, the overlap, total height and force values in each element can be determined at each position, and deployment can be simulated.

For a cylindrical Class-1 tensegrity structure with more than three struts in each stage, a similar procedure can be repeated to study the deployment. However, it is more difficult, even impossible, to determine the lengths of the saddle, vertical and diagonal cables to create the equilibrium matrix and obtain the non-trivial solutions analytically. Therefore, in order to study deployment of n-strut cylindrical Class-1 tensegrity booms, a generalization procedure is developed. Rather than seeking pure analytical solutions, numerical approaches in combination with symbolic manipulation are

used to address the deployment of generalized versions of n-strut cylindrical Class-1 tensegrity booms. The generalization procedure is achieved by defining nodal locations and connectivity in terms of a few parameters. The nodal coordinates and connectivity are found to follow a regular pattern and, accordingly, n-strut cylindrical Class-1 tensegrity booms can be constructed to study their deployment.

The nodal locations can be defined in terms of the length of struts, the overlap, the radii of circumscribing circles for the top and bottom levels, and the azimuth and declination angles. A key initial observation is that these nodes lie at a constant radius from the centerline on the xy plane, evenly spaced. For a two-stage example, on the z axis, the nodes are located on four different levels, as mentioned earlier. The pattern for defining the nodal locations is given in Table 1 and it is valid for all two-stage n-strut cylindrical Class-1 tensegrity booms.

Two-stage cylindrical Class-1 tensegrity booms have $4n$ nodes (n nodes in each level) and $10n$ elements. r_{base} is the radius of the circumscribing circles for the top and bottom levels, α_1 is the azimuth angle of the strut between nodes 1 and n+1, δ is the declination angle, l_b is the strut length, and h is the overlap. The azimuth angle of only one strut is sufficient to fully define the nodal locations as the orientations of struts are dependent on each other. Additionally, the angle γ is $\gamma = 2\pi/n$.

Connectivity information for an n-strut cylindrical Class-1 tensegrity boom is also required to fully define its configuration. A pattern is found to describe the connectivity between the nodes and, for clarity, a connectivity chart is generated as shown in Fig. 4.

In Fig. 4, each circle represents a node and the edge color of each circle defines the level the nodes belong to. Bottom, top, lower intersection, and upper intersection levels are indicated with black, blue, magenta, and red circles, respectively. Furthermore, the double-headed arrows indicate a connection between the associated nodes as well as the element type. Black, blue, magenta, teal, and red arrows represent top and bottom, vertical, saddle, diagonal cables, and struts, respectively. In order to avoid overlapping arrows in the connectivity chart, the first nodes of the bottom and top levels, i.e. 1 and $2n$+1, are located at the upper points of the corresponding layers while the

intersection layer is rotated approximately 60° in the counter-clockwise direction.

After defining the nodal locations and the connectivity information, the equilibrium matrix in Equation 2 can be generated using symbolic software. Since the nodal locations and element types are defined, the lengths of the saddle, vertical, and diagonal cables can be determined symbolically in terms of the parameters given in Table 1. The required derivatives can be taken, the equilibrium matrix can be formed and the determinant can be evaluated symbolically.

Non-trivial solutions to the prestressability conditions, Equation 3, are quadratic in overlap, h, and therefore, two solutions exist. These solutions can be evaluated for given values of r_{base} and l_b and they will depend only on α_1 and δ. These solutions are then evaluated for (α_1, δ) pairs and the overlap values are computed. For the obtained geometries, a force-finding method, developed by Tran and Lee (Tran and Lee 2010) is employed to determine the force densities carried by individual elements and to ensure that unilateral element behavior is satisfied, meaning that cables carry tension and struts carry compression. The (α_1, δ) pairs that satisfy unilateral element behavior are stored along with the corresponding overlap value (h). Finally, the collection of these points yields two equilibrium surfaces with respect to overlap and height, respectively. Then, deployment (increase of total height) can be achieved by varying the azimuth and declination angles while remaining on the equilibrium surface.

Cylindrical Class-1 tensegrity booms with more than two stages have been studied by several researchers (Nishimura 2000; Murakami and Nishimura 2001; Sultan and Skelton 2003). The form-finding problem for this type of structure is characterized by consistency equations for the intermediate and end stages separately, as a function of the number of struts, n, in each stage (Micheletti 2003). However, these consistency equations do not provide a general, straightforward deployment procedure similar to the approach using equilibrium surfaces described in this paper. The generalized deployment method presented here can be used for hybrid Class-1 and Class-2 tensegrity booms that are constructed by placing two cylindrical units of Class-1 tensegrity booms on top of another, creating a connection between struts at the nodes.

DEPLOYMENT OF CYLINDRICAL CLASS-2 TENSEGRITY BOOMS

Deployment of cylindrical Class-2 tensegrity booms is investigated by following two distinct deployment strategies. The first strategy involves the use of constant-length reinforcing cables while the second one utilizes variable-length reinforcing cables (or no reinforcing cables at all). The addition of reinforcing cables is optional and, when they are introduced to the structure, the overall stiffness of the structure will be improved and the twist angle will have a feasible range rather than a single value (Pinaud et al. 2004). The first strategy takes some advantage of the reinforcing cables without increasing the number of actuated cables.

Pinaud et al. (Pinaud et al. 2004) noted that the prestressability conditions for a three-strut cylindrical Class-2 tensegrity boom are satisfied if and only if the twist angle, α, between the two stacked tensegrity units is $\alpha = \pi/6$. Instead, the addition of reinforcing cables yields a feasible twist angle range of $\alpha = (\pi/6, \pi/2)$. The overall stiffness of the structure is also affected by the selection of the twist angle, which can be treated as a design variable for optimization purposes (Yildiz 2018).

The generalization of cylindrical Class-2 tensegrity booms is achieved in a way similar to the one used for the Class-1 case, by defining the nodal locations and determining the connections between the nodes. Similar patterns are identified for the nodal locations and connectivity, and these are again generalized using a table and a connectivity chart, which are valid for both of the aforementioned deployment strategies.

The nodal locations in this case can be defined in terms of the radii of the circumscribing circles for the bottom and top levels, the radius of the circumscribing circle for the intermediate level, the twist angle, the strut length, and the height of one stage. A key initial observation is that the nodes are evenly spaced along the edge of a circle in the xy plane at each level. For a two-stage example, on the z axis, the nodes are located on three different levels. The pattern for defining nodal locations is given in Table 2 and it is valid for two-stage, n-strut cylindrical Class-2 tensegrity booms.

Two-stage cylindrical Class-2 tensegrity booms have $3n$ nodes (n nodes in each level) and, depending on the incorporation of reinforcing cables, $7n$ or $9n$ elements. r_{base} is the radius of the

circumscribing circles for the top and bottom levels, r is the radius of the circumscribing circle for the intermediate level, α is the twist angle, l_b is the strut length, and h is the height of one stage. Without reinforcing cables, the twist angle must be $\alpha = \pi/2 - \pi/n$; however, the addition of reinforcing cables defines a feasible range for the twist angle, $\alpha = (\pi/2 - \pi/n, \pi/2)$. Additionally, the angle γ is $\gamma = 2\pi/n$.

Connectivity information for an n-strut cylindrical Class-2 tensegrity boom is also required to fully define its geometry. The pattern describing this is given with a connectivity chart and it is shown in Fig. 5.

In Fig. 5, each circle represents a node and the edge color of each circle defines the level the nodes belong to. Bottom, top, and intermediate levels are indicated with black, blue, and magenta circles. Furthermore, the double-headed arrows indicate a connection between the associated nodes and the element type. Black, blue, magenta, dashed orange, and red arrows represent top and bottom, vertical, saddle, reinforcing cables, and struts, respectively. In order to avoid overlapping arrows in the connectivity chart, the first nodes of the bottom and top levels, i.e. 1 and $2n$+1, are located at the upper point of the corresponding layer while the intermediate layer is rotated approximately 60° in the counter-clockwise direction.

In the following subsections, the deployment strategies are explained in further detail by using the nodal locations table and the connectivity chart.

Deployment with Constant Reinforcing Cables

This deployment strategy was studied by Pinaud et al. (Pinaud et al. 2004) for a triplex in an attempt to achieve deployment with improved stiffness by incorporating constant-length reinforcing cables. Since the lengths of the reinforcing cables were kept the same throughout the deployment, the required number of actuators does not increase. The main parameter controlling this deployment strategy is the twist angle, α, and it is varied to achieve deployment which involves a simultaneous rotation with extension. During deployment, as the structure extends r_{base} remains constant and r decreases.

Pinaud et al. (Pinaud et al. 2004) obtained expressions for the lengths of the saddle, vertical,

and reinforcing cables by calculating the distances between the associated nodes in the three-strut case. An expression for the length of the reinforcing cables can be obtained from the distance between nodes 2 and n+2, using the nodal locations defined in Table 2, as follows:

$$R = \sqrt{\Big(r\cos(\alpha) - r_{base}\cos(\gamma)\Big)^2 + \Big(r\sin(\alpha) - r_{base}\sin(\gamma)\Big)^2 + h^2} \tag{4}$$

Furthermore, a relationship between r and h can be formed as shown in Fig. 6, a perspective view of a strut, where a and b are two end nodes.

$$l_b^2 - h^2 = r_{base}^2 + r^2 - 2rr_{base}\cos(\gamma + \alpha) \tag{5}$$

Equation 4 can be solved, and solutions for r obtained as follows:

$$r = r_{base}\cos(\gamma + \alpha) \pm \sqrt{r_{base}^2\cos^2(\gamma + \alpha) + l_b^2 - h^2 - r_{base}^2} \tag{6}$$

Selection of the positive solution for r and its substitution into Equation 4, yields an expression for R, which is independent of the radius of the circumscribing circle for the intermediate level. Assuming a constant length for the reinforcing cables, R, a direct relationship between α and h can be formed.

Then, for given values of r_{base} and l_b, this relationship can be solved by using a Newton-Raphson Method for constant reinforcing cable length. The results can be represented by solution curves which represent how height of one stage varies with increasing twist angle in the feasible range. An issue encountered by Pinaud et al. with this deployment strategy is the potential collision of struts which takes place in the defined feasible range of the twist angle in the three-strut case. However, for tensegrity structures with more than three struts in each stage, this issue disappears (Yildiz 2018).

This deployment strategy is limited by the constant lengths of the reinforcing cables, and each solution curve has an inevitable upper limit. Increasing the twist angle beyond a certain value, the intermediate plane of the structure only rotates without achieving further deployment, a behavior

also observed by Pinaud et al. (Pinaud et al. 2004). Longer reinforcing cables allow longer booms to be designed, but the minimum height of the structure in the undeployed (stowed) configuration will also be greater.

Deployment with Variable Reinforcing Cables

The second deployment strategy for cylindrical Class-2 tensegrity booms can be used with or without reinforcing cables. In this deployment strategy, if reinforcing cables are not introduced, the twist angle must be set to $\alpha = \pi/2 - \pi/n$ in order to satisfy the prestressability condition. Alternatively, with variable-length reinforcing cables, the twist angle can be selected within the feasible range defined previously to pursue different goals, such as increased stiffness.

In this deployment strategy, the height of one stage, h, can be found by calculating the distance between two nodes, a and b, connected by a strut, as

$$h = \sqrt{l_b^2 - (x_a - x_b)^2 - (y_a - y_b)^2} \tag{7}$$

As the deployment proceeds, the height of one stage increases, affecting the node positions in the intermediate level. Since the x and y components of these nodes depend on each other through the radius of the circumscribing circle of the intermediate level, r can be determined from Equation 7 and Table 2. For any node located at the intermediate level, the x and y components can be related to r as follows:

$$x_i = r\cos(\beta_i) \qquad y_i = r\sin(\beta_i) \tag{8}$$

where β_i is the angle of each node measured counterclockwise from the x axis and it does not change during deployment.

In this way, it is possible to determine the position of each node at any instant during deployment by calculating the radius of the circumscribing circle of the intermediate level. For example, the strut between nodes 1 and n+3 (see Table 2) can be considered and the nodal locations can be used to establish a relationship between r and h through Equations 7 and 8.

In the next section, the strategies described here are applied to n-strut cylindrical Class-2 tensegrity booms to achieve deployment. Despite the increased number of actuators, the latter deployment strategy with reinforcing cables leads to better results since its use is not limited by the constant-length reinforcing cables and the stiffness is increased. Furthermore, the range of the first deployment strategy is limited by the constant-length reinforcing cables, and the maximum possible deployed heights cannot be reached.

DEPLOYMENT SIMULATIONS

In this section, the generalized deployment methods described above are used to simulate deployment of cylindrical Class-1 and Class-2 tensegrity booms. For demonstration and comparison purposes, the number of struts in each case is chosen as four ($n = 4$). In the deployment simulations, the bottom nodes are fixed while the others change their positions as the deployment proceeds. The cable-length and force-density (force per unit length) variations (found using the force-finding method (Tran and Lee 2010)) are tracked during deployment, and the results are presented.

In each deployment example, the radii of the circumscribing circles of the top and bottom levels, r_{base}, and the lengths of struts, l_b, are chosen to be $r_{base} = 0.156$ m and $l_b = 0.4$ m (consistent with the values used in (Sultan and Skelton 2003)).

Four-Strut Cylindrical Class-1 Tensegrity Boom

In this example, deployment of a two-stage four-strut cylindrical Class-1 tensegrity boom is simulated. For the given strut length and radii of the circumscribing circles and using the approach described in the preceding section, equilibrium surfaces are generated with respect to overlap and total height. These equilibrium surfaces are shown in Fig. 7.

For deployment simulation, the initial and final azimuth and declination angles are selected as $\alpha_{1,i} = 230°$, $\delta_i = 85°$, $\alpha_{1,f} = 210°$, and $\delta_f = 55°$. A linear deployment path is visualized with orange circles on the equilibrium surface with respect to total height, as shown in Fig. 7. Then, the deployment sequence is shown in Fig. 8. Furthermore, the force densities in each type of member are tracked by the force-finding method as the deployment proceeds. Fig. 9 shows the variations of

the lengths of the elements and the relative force densities in the elements, respectively. The force density in the top and bottom cables is held constant for comparison purposes.

Fig. 9(a) shows that the lengths of the top and bottom cables, as well as the struts, are constant while the lengths of all of the other elements (cables) are actively controlled. The vertical and diagonal cables are lengthened and the saddle cables are shortened to achieve deployment. Fig. 9(b) reveals that the cables are always in tension and the struts are in compression, satisfying unilateral element behavior throughout.

Four-Strut Cylindrical Class-2 Tensegrity Boom - Constant Reinforcing Cables

In this example, deployment of a two-stage four-strut cylindrical Class-2 tensegrity boom with constant-length reinforcing cables is simulated. Nodal locations are defined based on Table 2. Additionally, the full geometry of the structure is generated based on the connectivity chart given in Fig. 5.

Following these steps, the length of the reinforcing cables can be calculated symbolically using the nodal locations with Equation 4. Then, a similar relationship between the height of one stage and the radius of the circumscribing circle of the intermediate level is formed by Equation 5. The solutions to Equation 5 are found and the positive solution for r is substituted back into the expression for the reinforcing cable length obtained for four-strut cylindrical Class-2 tensegrity booms to establish a direct relationship between α and h. For constant R values, solution curves are obtained for the given r_{base} and l_b. These solution curves are shown in Fig. 10.

Then, the constant reinforcing cable length is selected as $R = 0.19$ m as it yields the maximum difference between the initial and final heights of one stage within the feasible twist angle range. The deployment is simulated by varying the twist angle between $\alpha_i = 48°$ and $\alpha_f = 81°$. The sequence of deployment can be seen in Fig. 11.

During the deployment, the lengths of each type of member and the force densities carried by these members are tracked. The variations of lengths and force densities are shown in Fig. 12. Fig. 12(a) shows that with the use of constant reinforcing cables, the deployment range is limited as the deployment continues with almost no extension in the total height during the final phase. This is

mainly due to the fact that as the deployment proceeds, the intermediate plane rotates and limits the achievable maximum height of one stage for a constant reinforcing cable length. Fig. 12(b) also shows that the cables carry tension, and the struts carry compression during deployment.

Four-Strut Cylindrical Class-2 Tensegrity Boom - Controlled Reinforcing Cables

In this example, deployment of a four-strut cylindrical Class-2 tensegrity boom is studied. For illustration purposes, reinforcing cables are introduced and they are actively controlled. As a result, there is no limitation on the deployment range of the structure since all cables including reinforcing ones are actively controlled. Nevertheless, the deployment range is practically limited by the decreasing radius of the circumscribing circle of the intermediate level.

The nodal locations and element connectivity are defined based on Table 2 and Fig. 5, respectively. The twist angle selection has a direct influence on the stiffness of the structure, as shown by Yildiz (Yildiz 2018), and can be determined based on different requirements. In this example, it is set to $\alpha = 3\pi/8$, which is in the feasible range of $(\pi/4, \pi/2)$. The height of one stage is related to the strut length and the radius of the circumscribing circle of the intermediate level through Equations 7 and 8.

The initial and final heights of one stage are selected as $h_i = 0.03$ m and $h_f = 0.26$ m, and the deployment is simulated. With this selected final deployed height, the tensegrity boom has a uniform cross-section in the fully-deployed configuration, which is not achievable using constant-length reinforcing cables. The deployment sequence is shown in Fig. 13.

Similarly, the lengths of each member are tracked and the force densities are calculated using the force finding method during deployment. Fig. 14 shows the variations of member lengths and force densities.

The results show that the deployment range is limited only by the radius of the circumscribing circle for the intermediate level. As the height of the structure increases, the radius of the intermediate level decreases to a nominal limit matching that of the top and bottom levels. Additionally, the force densities in the cables and struts are always positive and negative, respectively, meaning that unilateral element behavior is preserved during deployment.

CONCLUSIONS

This paper developed a general procedure for addressing deployment of n-strut cylindrical Class-1 and Class-2 tensegrity booms. The geometry and deployment behavior of three-strut cylindrical Class-1 and Class-2 tensegrity booms were described as a starting point. Generalization procedures were developed to investigate the deployment of cylindrical Class-1 and Class-2 tensegrity booms with more than three struts in each stage, a result not previously available in the literature. The generalization procedures start with defining the nodal locations in terms of a few parameters. Rotational symmetry and the regular polygons generated by the cylindrical tensegrity units enable the definition of nodal locations in terms of a few parameters, most importantly, the number of struts in each stage. In order to completely define the configurations, connectivity charts describing the connectivity between the nodes were developed.

For Class-1 tensegrity booms, a mixed symbolic-numerical approach was adopted to form the equilibrium matrix symbolically and obtain solutions to the prestressability conditions numerically. For Class-2 tensegrity booms, two different deployment strategies were investigated: one with constant-length reinforcing cables and another with variable-length reinforcing cables. The first deployment strategy involves a direct relationship between the height of one stage and the twist angle, and this relationship was numerically solved to yield solution curves. On the other hand, the second deployment strategy involves a relationship between the height of one stage and the radius of the circumscribing circle for the intermediate level.

Example deployment simulations for Class-1 and Class-2 tensegrity booms with four struts in each stage were examined. For comparison purposes, the radius of the top and bottom plane and the strut length were kept the same in all cases. During deployment, the lengths of each type of element were calculated and their variation was shown. Furthermore, the force-finding method was employed to track the force densities carried by different types of elements during deployment.

The simulations showed that Class-1 tensegrity structures can have very low initial heights, while that may be impractical for Class-2 tensegrity booms with constant-length reinforcing cables. On the other hand, both Class-1 tensegrity structures and Class-2 tensegrity structures with variable-length

reinforcing cables can be fully deployed to achieve a uniform boom cross-section. However, while Class-2 tensegrity booms with constant-length reinforcing cables have fewer actuators than Class-2 tensegrity booms with variable-length reinforcing cables, their deployment range is relatively limited.

The generalization procedures developed in this paper enable more straightforward design of deployable cylindrical Class-1 and Class-2 tensegrity booms. The number of struts can be increased arbitrarily for different purposes such as the pursuit of increased stiffness or stiffness-to-mass ratio. As a result, by varying the number of struts in each stage, the optimal design of tensegrity booms can be evaluated for potential use in future space missions. Other potential benefits of the generalization procedure may include increases in deployment/packaging efficiency and/or stiffness during deployment.

DATA AVAILABILITY STATEMENT

All data, models, and codes generated during this study are available from the corresponding author by request.

REFERENCES

Connelly, R. and Terrell, M. (1995). "Globally rigid symmetric tensegrities." *Structural Topology 1995 núm 21*.

Dalilsafaei, S., Eriksson, A., and Tibert, G. (2012). "Improving bending stiffness of tensegrity booms." *International Journal of Space Structures*, 27(2-3), 117–129.

Estrada, G. G. (2007). "Analytical and numerical investigations of form-finding methods for tensegrity structures." Ph.D. thesis, University of Stuttgart, Stuttgart, Germany.

Furuya, H. (1992). "Concept of deployable tensegrity structures in space application." *International Journal of Space Structures*, 7(2), 143–151.

González, A., Luo, A., and Shi, D. (2019). "Reconfiguration method of tensegrity units using infinitesimal mechanisms." *Engineering Computations*.

Guest, S. D. (2011). "The stiffness of tensegrity structures." *IMA Journal of Applied Mathematics*, 76(1), 57–66.

516 Hanaor, A. (1993). "Double-layer tensegrity grids as deployable structures." *International Journal*
517 *of Space Structures*, 8(1-2), 135–143.
518 Kebiche, K., Aoual, M. K., and Motro, R. (2008). "Continuum models for systems in a selfstress
519 state." *International Journal of Space Structures*, 23(2), 103–115.
520 Kebiche, K., Kazi-Aoual, M., and Motro, R. (1999). "Geometrical non-linear analysis of tensegrity
521 systems." *Engineering structures*, 21(9), 864–876.
522 Liu, M., Cao, D., and Zhu, D. (2019). "Equivalent dynamic model of the space antenna truss with
523 initial stress." *AIAA Journal*, 1–13.
524 Masic, M. and Skelton, R. (2003). "Open-loop shape control of stable unit tensegrity structures."
525 *Proceedings of the Third World Conference on Structural Control*, 439–447.
526 Masic, M., Skelton, R. E., and Gill, P. E. (2006). "Optimization of tensegrity structures." *Interna-*
527 *tional Journal of Solids and Structures*, 43(16), 4687–4703.
528 Micheletti, A. (2003). "The indeterminacy condition for tensegrity towers: A kinematic approach."
529 *Revue française de génie civil*, 7(3), 329–342.
530 Micheletti, A. and Williams, W. (2007). "A marching procedure for form-finding for tensegrity
531 structures." *Journal of mechanics of materials and structures*, 2(5), 857–882.
532 Motro, R. (2003). *Tensegrity: structural systems for the future*. Elsevier.
533 Murakami, H. (2001). "Static and dynamic analyses of tensegrity structures. part ii. quasi-static
534 analysis." *International Journal of Solids and Structures*, 38(20), 3615–3629.
535 Murakami, H. and Nishimura, Y. (2001). "Initial shape finding and modal analyses of cyclic
536 right-cylindrical tensegrity modules." *Computers & Structures*, 79(9), 891–917.
537 Murata, S., Jodoi, D., Furuya, H., Terada, Y., and Takadama, K. (2005). "Inflatable tensegrity
538 module for a large-scale space structure and its construction scenario." *The 56th International*
539 *Astronautical Congress (IAC05)*.
540 Nishimura, Y. (2000). "Static and dynamic analyses of tensegrity structures." Ph.D. thesis, Univer-
541 sity of California at San Diego, La Jolla, CA.
542 Pinaud, J.-P., Solari, S., and Skelton, R. E. (2004). "Deployment of a class 2 tensegrity boom."

543 *Smart Structures and Materials 2004: Smart Structures and Integrated Systems*, Vol. 5390,
544 International Society for Optics and Photonics, 155–163.
545 Pugh, A. (1976). *An introduction to tensegrity*. Univ of California Press.
546 Rhode-Barbarigos, L., Ali, N. B. H., Motro, R., and Smith, I. F. (2010). "Designing tensegrity
547 modules for pedestrian bridges." *Engineering Structures*, 32(4), 1158–1167.
548 Rhode-Barbarigos, L., Schulin, C., Ali, N. B. H., Motro, R., and Smith, I. F. (2012). "Mechanism-
549 based approach for the deployment of a tensegrity-ring module." *Journal of Structural Engineer-*
550 *ing*, 138(4), 539–548.
551 Russell, C. and Tibert, G. (2008). "Deployment simulations of inflatable tensegrity structures."
552 *International Journal of Space Structures*, 23(2), 63–77.
553 Skelton, R. E. and de Oliveira, M. C. (2009). *Tensegrity systems*, Vol. 1. Springer.
554 Sultan, C. (2014). "Tensegrity deployment using infinitesimal mechanisms." *International Journal*
555 *of Solids and Structures*, 51(21-22), 3653–3668.
556 Sultan, C. and Skelton, R. (2003). "Deployment of tensegrity structures." *International Journal of*
557 *Solids and Structures*, 40(18), 4637–4657.
558 Sultan, C. and Skelton, R. T. (1998). "Tendon control deployment of tensegrity structures." *Smart*
559 *Structures and Materials 1998: Mathematics and Control in Smart Structures*, Vol. 3323,
560 International Society for Optics and Photonics, 455–467.
561 Sychterz, A. C. and Smith, I. F. (2017). "Joint friction during deployment of a near-full-scale
562 tensegrity footbridge." *Journal of Structural Engineering*, 143(9), 04017081.
563 Tibert, G. and Pellegrino, S. (2003). "Deployable tensegrity masts." *44th*
564 *AIAA/ASME/ASCE/AHS/ASC Structures, Structural Dynamics, and Materials Conference*,
565 1978.
566 Tran, H. C. and Lee, J. (2010). "Initial self-stress design of tensegrity grid structures." *Computers*
567 *& structures*, 88(9-10), 558–566.
568 Vu, K., Liew, J. R., and Anandasivam, K. (2006). "Deployable tension-strut structures: from
569 concept to implementation." *Journal of Constructional Steel Research*, 62(3), 195–209.

570 Yildiz, K. (2018). “Cable actuated tensegrity structures for deployable space booms with enhanced
571 stiffness.” Ph.D. thesis, The Pennsylvania State University, University Park, PA.
572 Yildiz, K. and Lesieutre, G. A. (2019). “Effective beam stiffness properties of n-strut cylindrical
573 tensegrity towers.” *AIAA Journal*, 57(5), 2185–2194.

List of Tables

TABLE 1. Locations of the nodes in a two-stage n-strut cylindrical Class-1 tensegrity boom

	Node	x	y	z
Bottom Level	1	r_{base}	0	0
	2	$r_{base}\cos(\gamma)$	$r_{base}\sin(\gamma)$	0
	3	$r_{base}\cos(2\gamma)$	$r_{base}\sin(2\gamma)$	0
	$\cdots$	$\cdots$	$\cdots$	0
	n-1	$r_{base}\cos((n-2)\gamma)$	$r_{base}\sin((n-2)\gamma)$	0
	n	$r_{base}\cos((n-1)\gamma)$	$r_{base}\sin((n-1)\gamma)$	0
Upper Intersection Level	n+1	$x_1 + l_b\cos(\alpha_1)\sin(\delta)$	$y_1 + l_b\sin(\alpha_1)\sin(\delta)$	$l_b\cos(\delta)$
	n+2	$x_2 + l_b\cos(\alpha_1+\gamma)\sin(\delta)$	$y_2 + l_b\sin(\alpha_1+\gamma)\sin(\delta)$	$l_b\cos(\delta)$
	n+3	$x_3 + l_b\cos(\alpha_1+2\gamma)\sin(\delta)$	$y_3 + l_b\sin(\alpha_1+2\gamma)\sin(\delta)$	$l_b\cos(\delta)$
	$\cdots$	$\cdots$	$\cdots$	$l_b\cos(\delta)$
	2n-1	$x_{n-1} + l_b\cos(\alpha_1+(n-2)\gamma)\sin(\delta)$	$y_{n-1} + l_b\sin(\alpha_1+(n-2)\gamma)\sin(\delta)$	$l_b\cos(\delta)$
	2n	$x_n + l_b\cos(\alpha_1+(n-1)\gamma)\sin(\delta)$	$y_n + l_b\sin(\alpha_1+(n-1)\gamma)\sin(\delta)$	$l_b\cos(\delta)$
Top Level	2n+1	$r_{base}\cos(\gamma/2)$	$r_{base}\sin(\gamma/2)$	$2l_b\cos(\delta)-h$
	2n+2	$r_{base}\cos(\gamma/2+\gamma)$	$r_{base}\sin(\gamma/2+\gamma)$	$2l_b\cos(\delta)-h$
	2n+3	$r_{base}\cos(\gamma/2+2\gamma)$	$r_{base}\sin(\gamma/2+2\gamma)$	$2l_b\cos(\delta)-h$
	$\cdots$	$\cdots$	$\cdots$	$2l_b\cos(\delta)-h$
	3n-1	$r_{base}\cos(\gamma/2+(n-2)\gamma)$	$r_{base}\sin(\gamma/2+(n-2)\gamma)$	$2l_b\cos(\delta)-h$
	3n	$r_{base}\cos(\gamma/2+(n-1)\gamma)$	$r_{base}\sin(\gamma/2+(n-1)\gamma)$	$2l_b\cos(\delta)-h$
Lower Intersection Level	3n+1	$x_{2n+1} + l_b\cos(\alpha_1+\gamma/2)\sin(\delta)$	$y_{2n+1} + l_b\sin(\alpha_1+\gamma/2)\sin(\delta)$	$l_b\cos(\delta)-h$
	3n+2	$x_{2n+2} + l_b\cos(\alpha_1+\gamma+\gamma/2)\sin(\delta)$	$y_{2n+2} + l_b\sin(\alpha_1+\gamma+\gamma/2)\sin(\delta)$	$l_b\cos(\delta)-h$
	3n+3	$x_{2n+3} + l_b\cos(\alpha_1+2\gamma+\gamma/2)\sin(\delta)$	$y_{2n+3} + l_b\sin(\alpha_1+2\gamma+\gamma/2)\sin(\delta)$	$l_b\cos(\delta)-h$
	$\cdots$	$\cdots$	$\cdots$	$l_b\cos(\delta)-h$
	4n-1	$x_{3n-1} + l_b\cos(\alpha_1+(n-2)\gamma+\gamma/2)\sin(\delta)$	$y_{3n-1} + l_b\sin(\alpha_1+(n-2)\gamma+\gamma/2)\sin(\delta)$	$l_b\cos(\delta)-h$
	4n	$x_{3n} + l_b\cos(\alpha_1+(n-1)\gamma+\gamma/2)\sin(\delta)$	$y_{3n} + l_b\sin(\alpha_1+(n-1)\gamma+\gamma/2)\sin(\delta)$	$l_b\cos(\delta)-h$

TABLE 2. Locations of the nodes in a two-stage n-strut cylindrical Class-2 tensegrity boom

	Node	x	y	z
Bottom Level	1	r_{base}	0	0
	2	$r_{base}\cos(\gamma)$	$r_{base}\sin(\gamma)$	0
	3	$r_{base}\cos(2\gamma)$	$r_{base}\sin(2\gamma)$	0
	$\cdots$	$\cdots$	$\cdots$	0
	n-1	$r_{base}\cos((n-2)\gamma)$	$r_{base}\sin((n-2)\gamma)$	0
	n	$r_{base}\cos((n-1)\gamma)$	$r_{base}\sin((n-1)\gamma)$	0
Intermediate Level	n+1	$r\cos(\alpha-\gamma)$	$r\sin(\alpha-\gamma)$	h
	n+2	$r\cos(\alpha)$	$r\sin(\alpha)$	h
	n+3	$r\cos(\alpha+\gamma)$	$r\sin(\alpha+\gamma)$	h
	$\cdots$	$\cdots$	$\cdots$	h
	$2n$-1	$r\cos(\alpha+(n-3)\gamma)$	$r\sin(\alpha+(n-3)\gamma)$	h
	$2n$	$r\cos(\alpha+(n-2)\gamma)$	$r\sin(\alpha+(n-2)\gamma)$	h
Top Level	$2n$+1	r_{base}	0	$2h$
	$2n$+2	$r_{base}\cos(\gamma)$	$r_{base}\sin(\gamma)$	$2h$
	$2n$+3	$r_{base}\cos(2\gamma)$	$r_{base}\sin(2\gamma)$	$2h$
	$\cdots$	$\cdots$	$\cdots$	$2h$
	$3n$-1	$r_{base}\cos((n-2)\gamma)$	$r_{base}\sin((n-2)\gamma)$	$2h$
	$3n$	$r_{base}\cos((n-1)\gamma)$	$r_{base}\sin((n-1)\gamma)$	$2h$

List of Figures

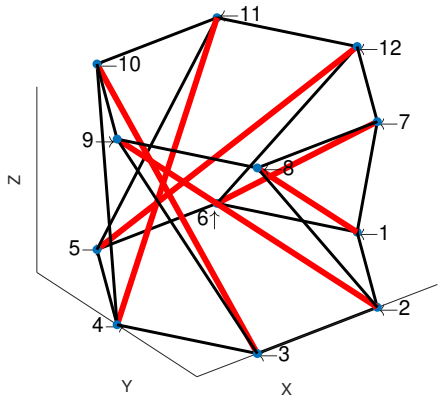

Fig. 1. Six-strut cylindrical tensegrity unit, Hexaplex

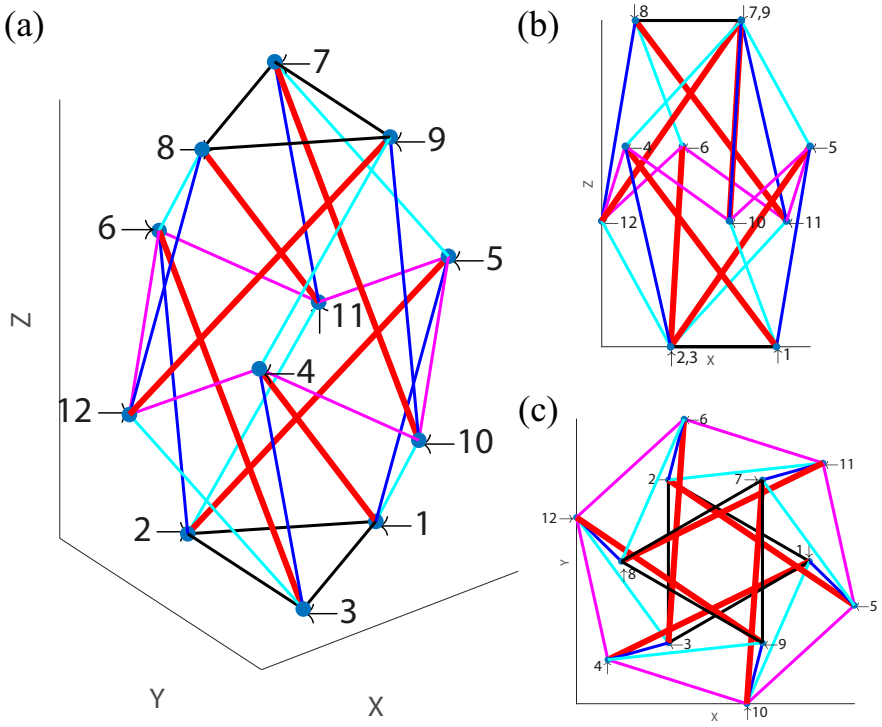

Fig. 2. Two-stage three-strut cylindrical Class-1 tensegrity boom (a) perspective, (b) top, and (c) side views

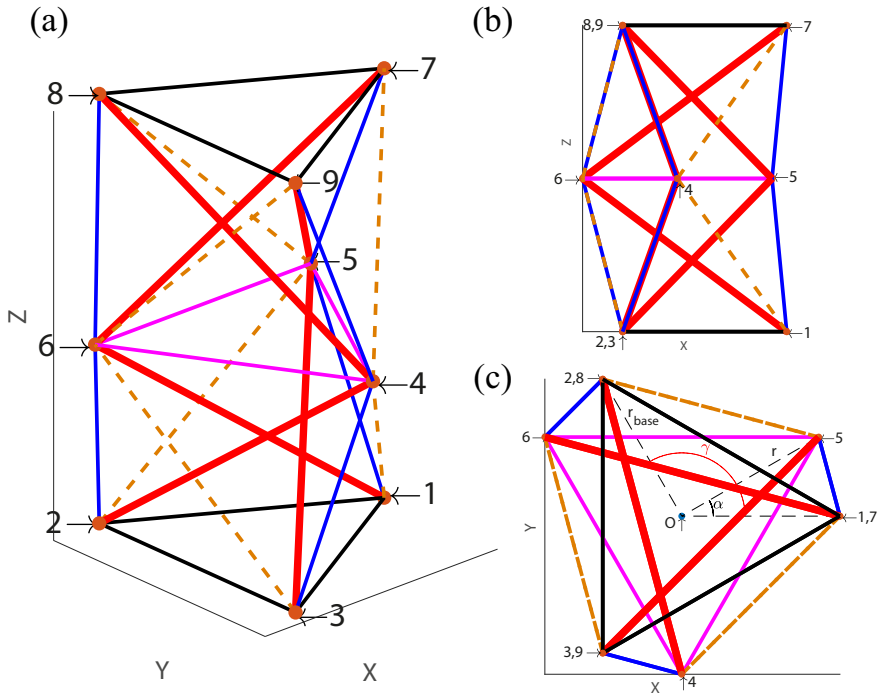

Fig. 3. Two-stage three-strut cylindrical Class-2 tensegrity boom (a) perspective, (b) top, and (c) side views

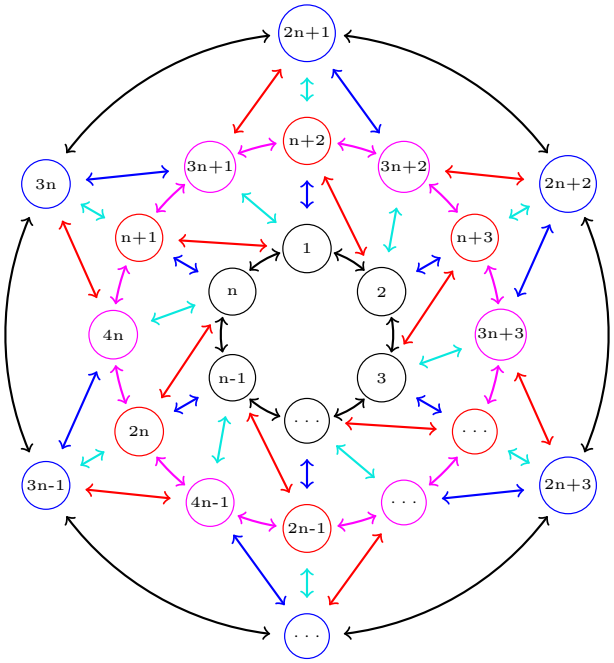

Fig. 4. Connectivity chart for two-stage cylindrical Class-1 tensegrity booms

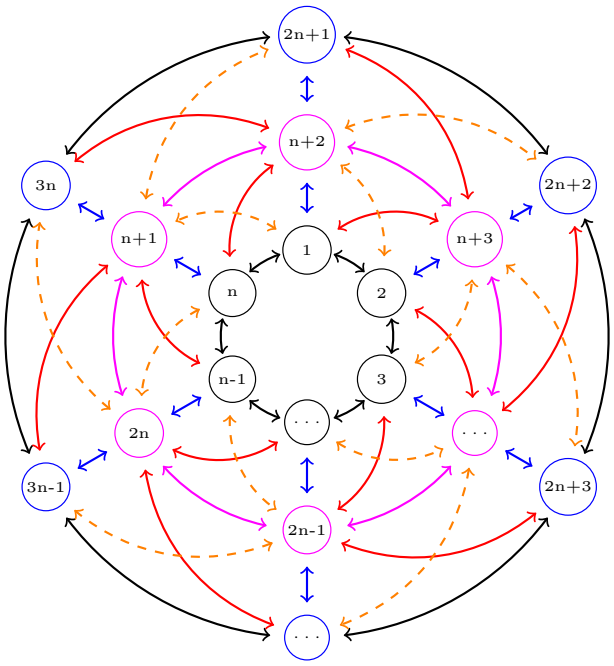

Fig. 5. Connectivity chart for two-stage cylindrical Class-2 tensegrity booms

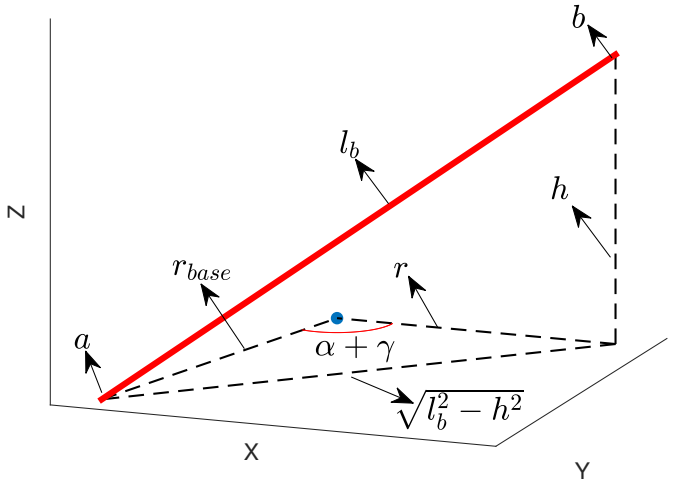

Fig. 6. Perspective view of a strut

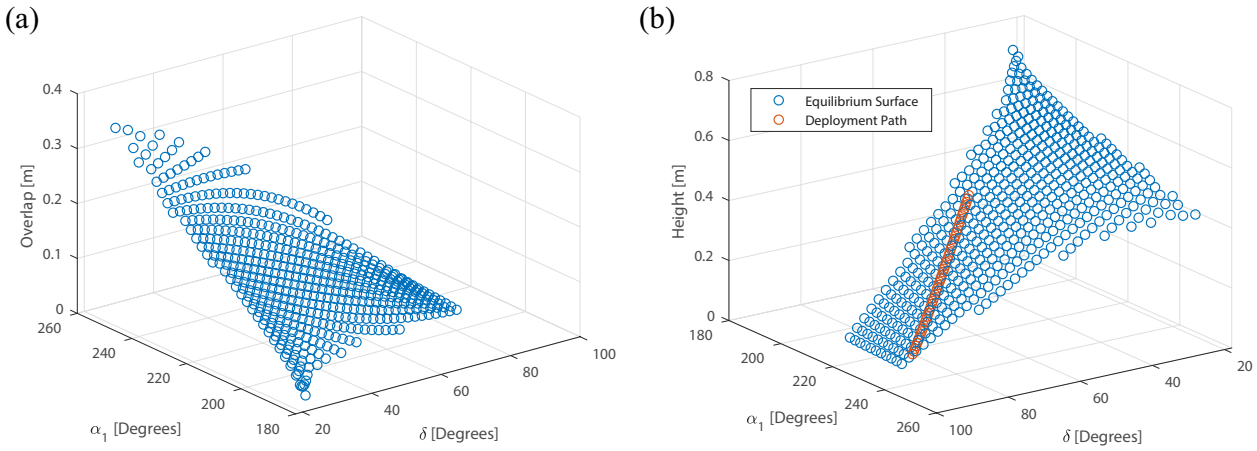

Fig. 7. The equilibrium surface with respect to (a) overlap and (b) total height

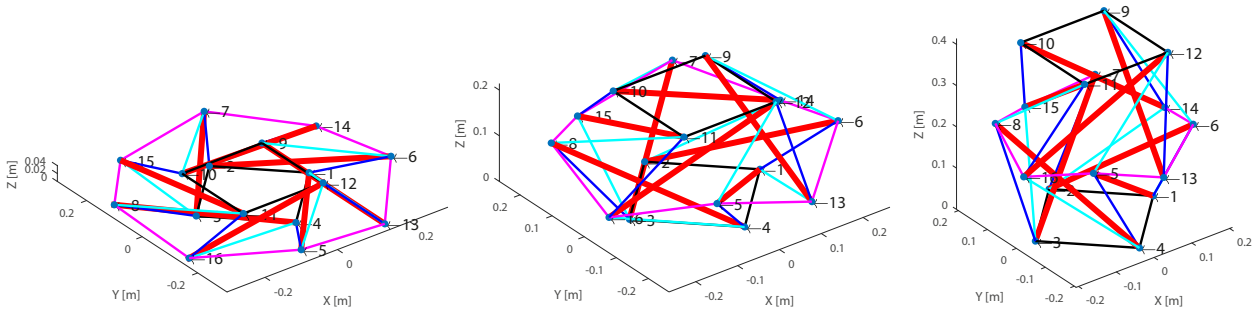

Fig. 8. The deployment sequence of the four-strut cylindrical Class-1 tensegrity boom

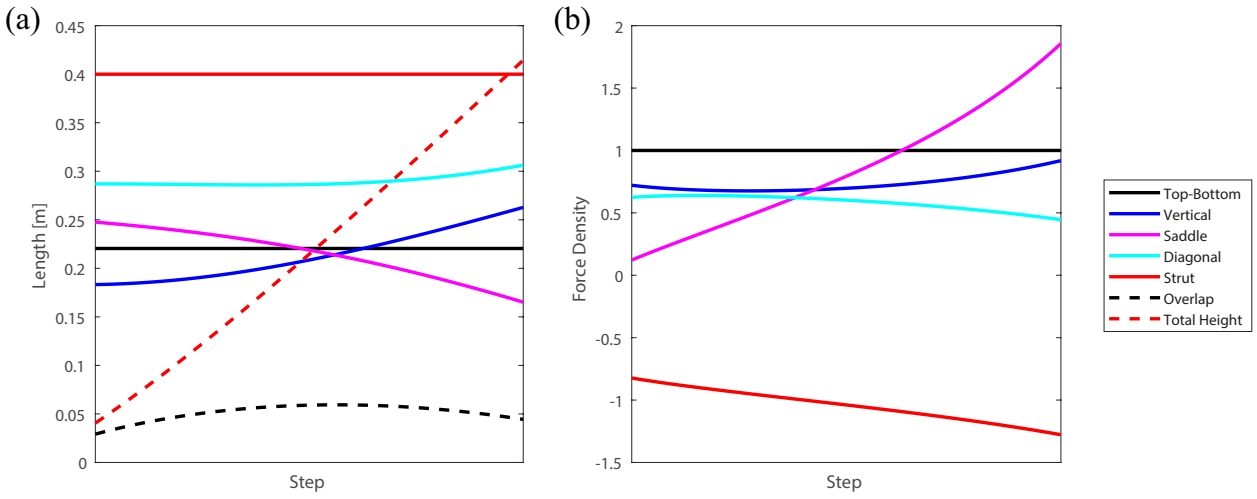

Fig. 9. Variation of (a) member lengths and (b) force densities

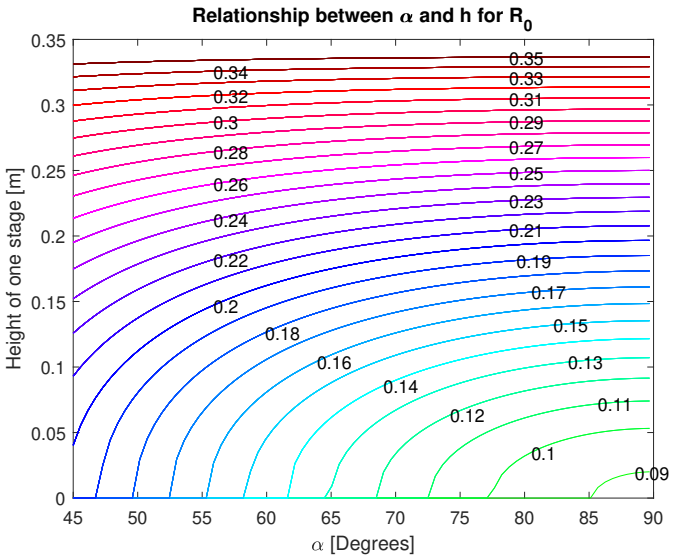

Fig. 10. The relationship between α and h (Contours are for constant R)

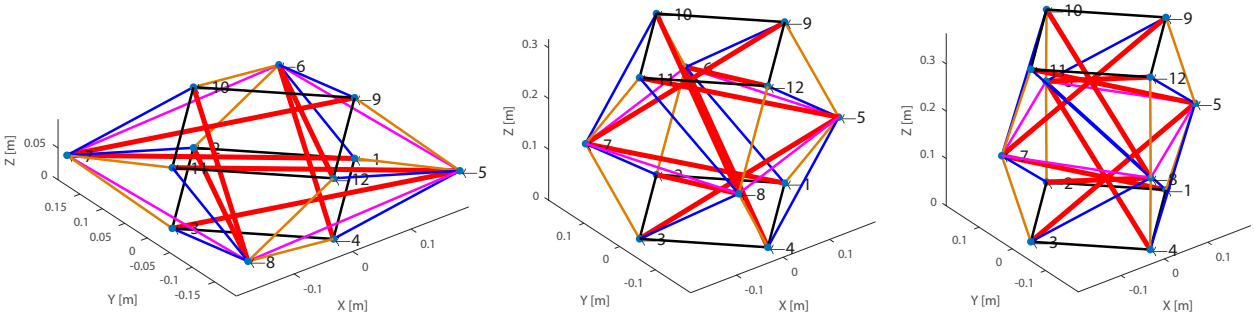

Fig. 11. The deployment sequence of the four-strut cylindrical Class-2 tensegrity boom with constant reinforcing cables

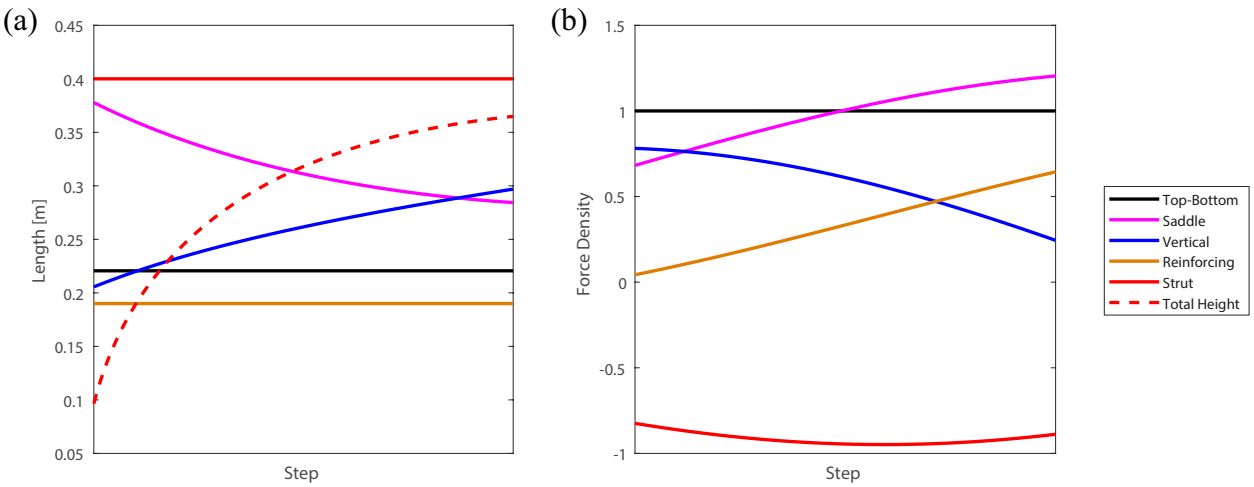

Fig. 12. Variation of (a) member lengths and (b) force densities

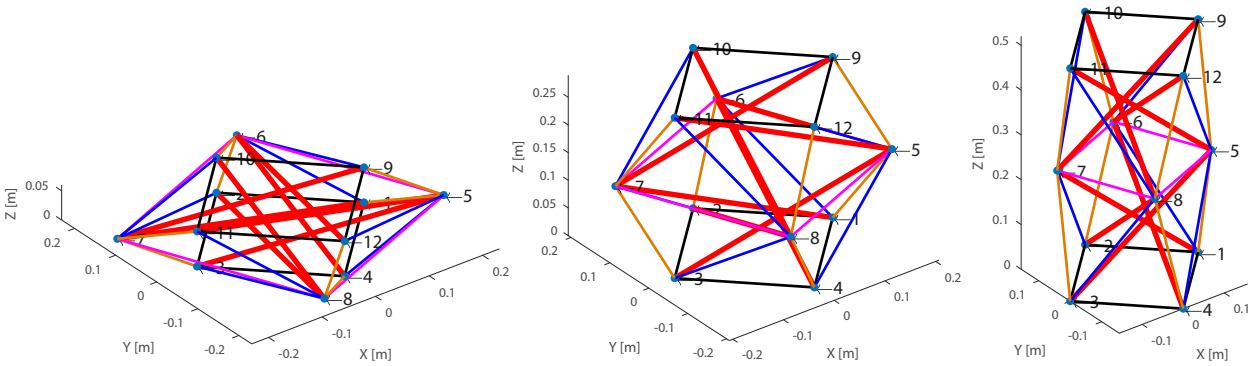

Fig. 13. The deployment sequence of the four-strut cylindrical Class-2 tensegrity boom with varying reinforcing cables

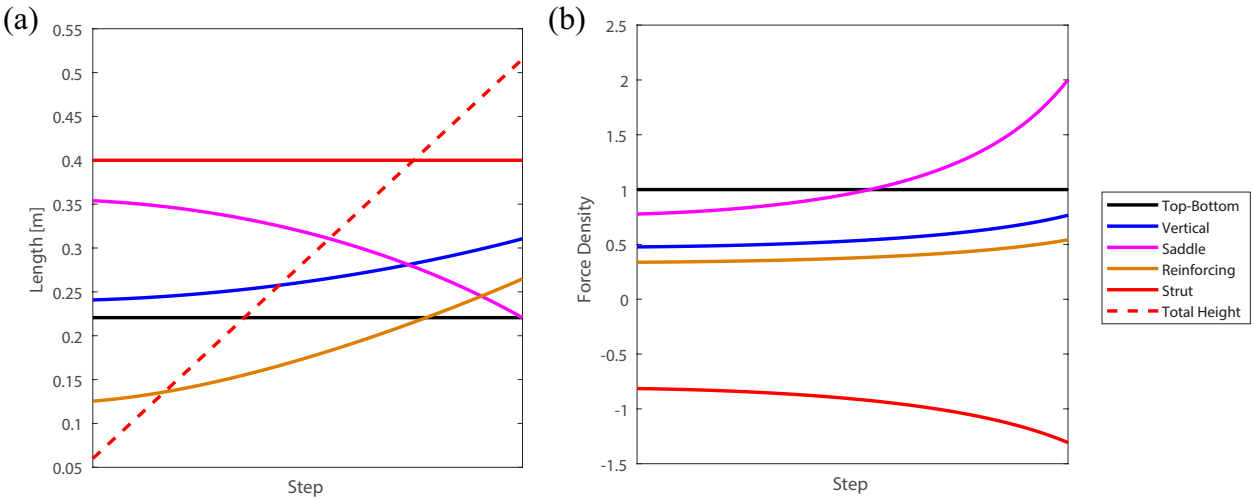

Fig. 14. Variation of (a) member lengths and (b) force densities